RSC Advances

PAPER

View Article Online
View Journal | View Issue

Cite this: *RSC Adv.*, 2023, **13**, 3575

Smartphone-assisted microfluidic and spectrophotometric recognition of hydrazine: a new platform towards rapid analysis of carcinogenic agents and environmental technology†

Kambiz Ghaseminasab,[a] Nastaran Aletaha[bc] and Mohammad Hasanzadeh *[ad]

Hydrazine (Hyd), a poisonous substance, is frequently employed in agriculture and industry as a scavenger to remove residues of oxygen from boiler feed water, electrical power plants, *etc.* Even at trace amounts, these chemicals are hazardous to humans. To limit the risks of exposure, there is a critical need for sensors for the monitoring of Hyd concentration to guarantee they are below harmful levels. In comparison to other approaches, the colorimetric method has garnered a great deal of interest due to its high sensitivity, speed, convenience, and simple optical color change detection. This study's primary purpose is to develop a portable tool for the colorimetric and spectrophotometric detection of Hyd using silver nanoparticles (silver nanoprism (AgNPr), silver nanowires (AgNW), and silver citrate (AgCit)). In addition, UV-visible spectroscopy was utilized for the quantitation evaluation of Hyd in real samples. The proposed approach demonstrated a linear range of 0.08 M to 6 M for Hyd by AgNW and 0.02 to 5 M by AgNPr as optical probes, whereas AgCit exhibited no color change (negative response). Using AgNPr and AgNW, the low limit of detection of Hyd was 200 μM and 800 μM, respectively. In addition, a novel method was employed for the first time to explore the effect of time on the determination of the candidate analyte. Consequently, the proposed method can be utilized to detect Hyd in real samples. Therefore, our method shows both qualitative and quantitative measurement of Hyd with high sensitivity, low cost, and fast analysis time and promisingly it can be industrialized for quick detection of Hyd in aquatic real samples.

Received 5th December 2022
Accepted 13th January 2023

DOI: 10.1039/d2ra07761b

rsc.li/rsc-advances

1. Introduction

Hydrazine (Hyd) is a chemical molecule that has several industrial uses, including for pipelines, missile fuel, protective coatings for boilers, fuel cell technology, and photographic reagents.[1,2] In addition, it has been used in pharmaceutical precursors, catalytic reagents, and agricultural compounds.[3,4] Hydrazine is poisonous and carcinogenic to the human body, and long-term exposure can cause damage to the lungs, liver, brain, and kidneys, among other significant consequences.[5] Various methods of hydrazine leakage from industrial sites into aquatic environments have been documented.[1,6] It's noteworthy that hydrazine breaks down in the soil through oxidation at a quicker rate than in water systems. Furthermore, the half-time of hydrazine in rivers or lakes is usually up to 250 days and it tends to be harmful to various microorganisms once it is present in high volumes.[7,8] Therefore monitoring of this target in real samples is very important and different methods are available for detection of hydrazine in environmental materials such as, chemiluminescence, spectrophotometry,[9] and fluorescence,[10] which are a few of the most common ones used today.[11,12] In most cases, these techniques frequently are employed, but they have a number of drawbacks, such as high operating cost, time-consuming process and requiring bulky equipment. However, colorimetric approaches have given a speedy, cost-effective, straightforward, and sensitive method for real-time tracking.[13,14]

According to the benefits of Ag nanoparticles such as easy manufacture, low cost, high surface area, excellent stability, variable composition and structure, tunable catalytic activity, and strong electrical conductivity; these nanomaterials are now a crucial and great optical candidate for colorimetric analysis, biomedical/environmental science and microfluidic technology.[15–18]

[a]*Pharmaceutical Analysis Research Center, Tabriz University of Medical Sciences, Tabriz, Iran. E-mail: hasanzadehm@tbzmed.ac.ir*

[b]*Food and Drug Safety Research Center, Tabriz University of Medical Sciences, Tabriz, Iran*

[c]*Biotechnology Research Center, Tabriz University of Medical Sciences, Tabriz, Iran*

[d]*Nutrition Research Center, Tabriz University of Medical Sciences, Tabriz, Iran*

† Electronic supplementary information (ESI) available. See DOI: https://doi.org/10.1039/d2ra07761b

Recently, microfluidic paper-based analytical devices (μPADs) have exhibited a strong desire to be utilized in several analytical detection and sensing devices. Typically, the manufacture of μPADs requires hydrophobic boundaries on the surface to define fluid flow patterns.[19] The hydrophilic characteristic of paper induces horizontal flow movement and, thus, fluid transfer inside the paper's high porosity.[20,21] Various processes, including laser cutting, wax printing, screen printing, and polydimethylsiloxane (PDMS) plotting, can be used to build hydrophobic barriers. One of the popular and famous methods is using a printer to make a particular pattern on the wax screen and PDMS (polydimethylsiloxane). Traditional microfluidics is made of glass, silicon, and polymers (such as PDMS (polydimethylsiloxane) and poly(methyl methacrylate) (PMMA)) and requires a cleanroom to build. But, the use of these techniques/materials is costly and requires advanced devices and equipment. Interestingly paper-based microfluidics is made from affordable materials and does not require a cleanroom or computer-controlled pumps to operate. These features make paper microfluidics the ideal medium for developing point-of-care diagnostic tests in all areas.

On the other hand, different monitoring technologies, such as electrochemical, chemiluminescence, colorimetric, and, mass spectrometry techniques, have been investigated in conjunction with the use of paper-based sensors.[22] The colorimetric test has been considered of the most advantageous identification techniques due to its mobility and simplicity of detection.[22] Microfluidic paper-based colorimetric devices (μPCD) rely on a change in color caused by the presence of target analytes; the interaction between the μPCD level and the target analyte determines the device's sensitivity and its ability to be applied for the analytical studies. The results can be understood just by naked eye.[23,24]

Given the drawbacks of conventional techniques, colorimetric sensors were created in this work to detect hydrazine in aqueous solution and establish outstanding sensitivity as well as other analytical criteria. Then, a colorimetric chemosensor based on AgNPs was used to identification of hydrazine in real samples. The final step was to demonstrate potential applications (μPCDs) toward analytical studies.[23,25,26]

In this study, for the first time, μPCD was decorated by silver nanoprism (AgNPr), silver nanowires (AgNW), and silver citrate (AgCit) and applied for the detection of hydrazine. Also, through UV-visible spectroscopy quantitative analysis of hydrazine without the requirement for any extra reagents and pretreatment was performed. Our constructed μPCDs function by changing the color of the sensing probe in the presence of analyte. Additionally, we used several types of AgNPs with different morphology to selectively detect hydrazine among other interfering agents (metal ions and organic chemicals) leading to observable changes in optical and color properties, which were further confirmed using the UV-visible spectroscopy technique. Through the use of a unique chemo-sensor and μPCDs, the specific colorimetric response of hydrazine among the other compounds found in real environmental samples enables exceptional selectivity for this analyte to be distinguished with the naked eye in this work. Finally, the main goal of this work is to propose an appropriate portable tool for colorimetric recognition of hydrazine using μPCD decorated by AgNPs.

2. Experimental

2.1. Chemicals and materials

For this experiment, utilized chemicals purchased from Sigma Aldrich (Ontario, Canada): hydrazine monohydrate (80%), silver nitrate ($AgNO_3$), hydrogen peroxide (H_2O_2, 30 wt%), sodium borohydride ($NaBH_4$, 96%), PVP K30 (polyvinyl pyrrolidone), acetic acid (CH_3COOH), triethylamine ($C_6H_{15}N$), potassium iodide (KI), hydrogen tetrachlorocuprate. Ethylene glycol (EG), methanol, ethanol, formaldehyde, acetone and glucose (Glu) were obtained from Merck (Germany). The standard solutions of Na^+, K^+, and Ca^{2+} were provided from chemlab company (Zedelgem, Belgium).

2.2. Instrumentation

To analyze the size distribution and assess the zeta potential of the produced silver nanoparticles, we used Zetasizer Ver. 7.11 (Malvern Instruments Ltd, MAL1032660, England) for dynamic light scattering (DLS) analysis. High-resolution field-emission scanning electron microscopy (FE-SEM, Hitachi-Su8020, Czech) at 3 kV was used to evaluate the surface morphology of nanoparticles, and energy-dispersive spectroscopy (EDS) was used in tandem with the FE-SEM to determine the nanoparticles' chemical compositions. To measure the dynamic size of the produced nanoparticles, Nanosurf (AG Gräubernstrasse 124 410 Liestal Switzerland) used an atomic force microscope (AFM) in a tapping mode. Additionally, in this investigation, the size and morphology of synthesis materials were analyzed using a transmission electron microscope (TEM) from Adelaide, Australia, operating at a voltage of 200 kV. colorimetric identification was carried out with the camera (Samsung SM-N920C smartphone, 600-dpi resolution). The images were recorded under natural or flasher light sources.

2.3. Preparation of super-hydrophobic paper-based microfluidic device

A metal design and paraffin are applied to a paper substrate (TLC and fiberglass paper) to create the μPCD. Paraffin was used because of its benefits, including its low melting point, inexpensive cost, and thermoplastic characteristics. Furthermore, paraffin, a key ingredient in solid ink, is frequently employed in the production of μPCDs in the wax printing method and is resistant to the majority of the chemical compounds used in the study. The proposed pattern consists of eight hydrophilic circular zones. Five-millimeter-diameter circular diagnostic zones are coupled with ten-millimeter-long and thirty-millimeter-wide microfluidic channels and a ten-millimeter-diameter central zone for the inlet sample. This paper describes the formation of hydrophilic regions and the preparation of μPCD. To achieve this, the candle was first melted at a temperature of 90 °C, and then the appropriate paper floated in it for 30 seconds. After drying, the iron pattern was heated for

Scheme 1 The fabrication process of paper-based microfluidic device, (A) materials and equipment required (B) immersion of fiberglass paper in molten paraffin at 90 °C, (C) dry paraffin-impregnated paper at room temperature, (D) place paraffin-free paper between paraffin-containing paper and a magnet, (E) place paraffin paper on the paraffin-free paper (F) place paraffin-free paper and paraffin-containing paper between the iron pattern and the magnet, (G) attract the pattern to the magnet (H) separation of pattern and magnet (I) formation of microfluidic channels in paraffin-free paper, (J) made paper-based microfluidic device.

two minutes at 150 °C. Between the iron design and the magnet has placed a sheet of paper. As a result, the paraffin penetrated into the paper's structure and formed hydrophilic channels on the surface. The prepared μPCD after drying was utilized for colorimetric analyses (Scheme 1 and S1 (see ESI†)).[27,28]

Hydrazine was discovered using μPCD modified by optical nano-probes (AgNPrs and AgNWs). For the decoration of detection zones, one droplet of probes was immobilized and dried at room temperature. Therefore, the suggested method is a step toward the creation of hydrazine diagnostic kits that are qualitatively superior and can change color quickly and inexpensively. In order to determine LOD and other relevant parameters, two types of AgNPs were employed for hydrazine monitoring were examined initially in solution in this research. Real aquatic samples were also used, and then paper devices (μPCDs) were employed to demonstrate potential future uses. For better understanding the procedure is summarized in Scheme 2.

2.4. Synthesis of various type of AgNPs with different size and morphology

2.4.1. Ag nanoprism (Ag NPrs). Initially, a PVP solution (0.06 g PVP in 3 mL) was added to 200 mL of water in order to synthesize Ag NPrs. Then, a solution of $AgNO_3$ (0.01 M, 4 mL) was added and agitated. TCS solution (75 mM, 8 mL) was added to the mixture, followed by the addition and stirring of 1 L of hydrogen peroxide. Afterward, a 100 mM by 3.2 L of $NaBH_4$ solution was added to the combination. The use of $NaBH_4$ as a reducing agent result in the creation of tiny Ag NPrs and a strong yellow coloring of the solution. After a few seconds, the color of the colloidal solution changed to pale yellow. After 30 minutes of stirring at room temperature, the hue of the resultant liquid changed to blue. The resulting colloidal mixture was kept at 4 °C for future use.

2.4.2. Ag nanowires (Ag NWs). To create Ag NWs, PVP (0.668 g) and ethylene glycol (EG) (20 mL) were combined and agitated at 170 °C for 20 to 30 minutes. 0.05 g of finely chopped silver chloride (AgCl) was added and agitated for three minutes

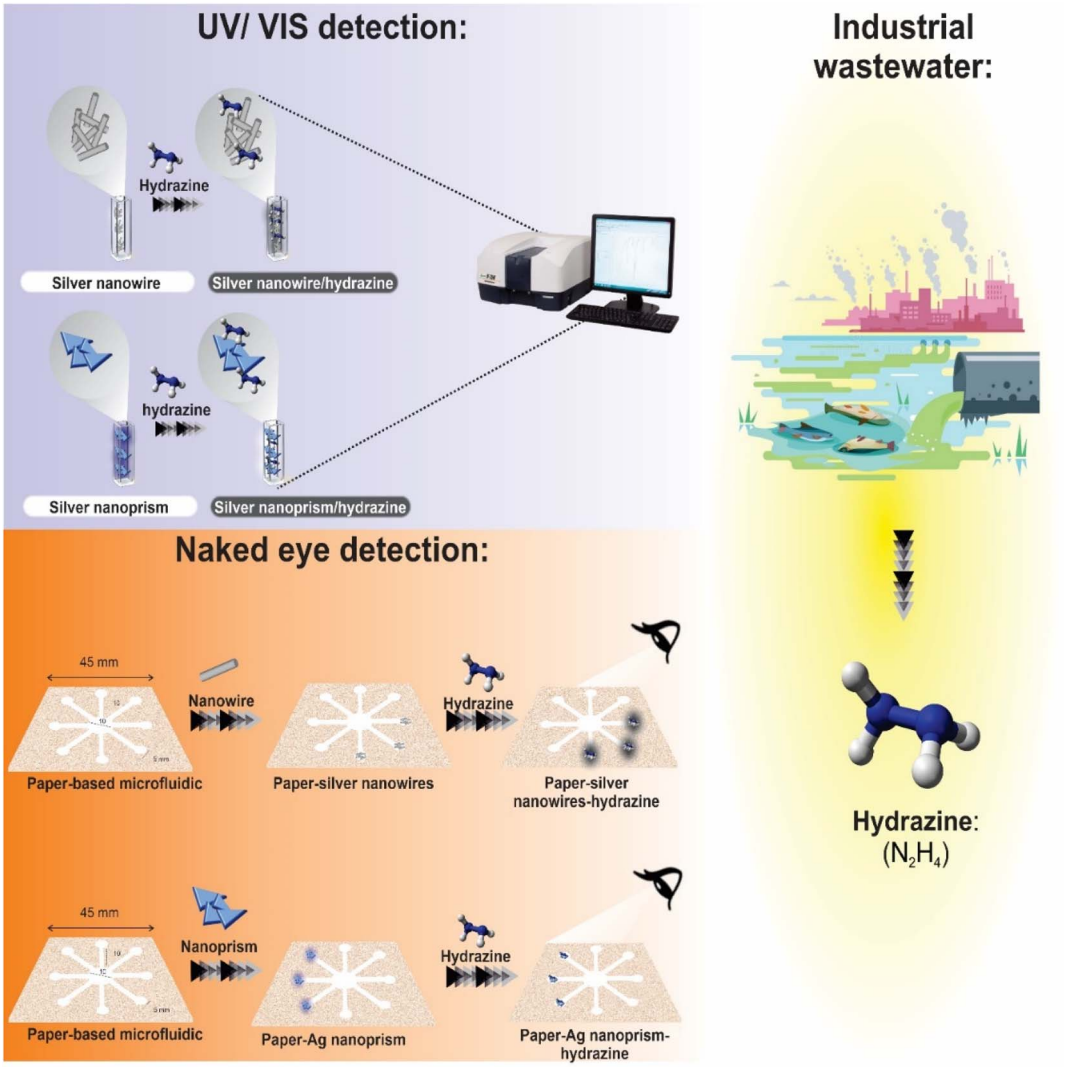

Scheme 2 Schematic illustration for the detection of hydrazine in real samples through UV-visible spectroscopy and μPCD colorimetric assays.

at the same temperature in order to make the seed. Next, silver nitrate ($AgNO_3$) (0.22 g per 10 mL of EG) was added to the mixture to generate nanowires. To finish the growth, 30 minutes of heating at 170 °C were required. After cooling, it was centrifuged for 30 minutes at 6000 rpm with methanol to remove PVP, EG, and other impurities.

2.4.3. Ag citrate (Ag Cit). First, a bath of cold water was prepared. Next, 400 mL of $Na_3C_6H_5O_7$ (1.06 mM) solution was thoroughly combined with 25 mL of $AgNO_3$ (5 μm) solution, and the mixture was agitated in an ice water bath. Then, 2.5 L of a freshly produced $NaBH_4$ (100 mM) solution was added drop by drop. The hue of the solution transforms from colorless to pale yellow. The solution was then agitated in the dark for around 120 minutes until a bright yellow tint became evident. The nanoparticles that were synthesized were spun at 6000 rpm for 15 minutes at room temperature.

3. Results and discussion

3.1. Characterization

3.1.1. Ag nanoprism (Ag NPrs). In proportion to their size, shape, and size distribution, silver noble metal nanoparticles exhibit optical characteristics that are unique and modifiable. AgNPrs were produced, and their TEM was recorded. According to (Fig. S1 (see ESI†)), the TEM images of nanoparticles were triangular. DLS was used to measure the distribution of charge and particle size. As shown in Fig. S2 (see ESI†), the average particle size per nanoparticle is 0.78 nm. To study the changes in nanoparticle size in the reaction system, DLS measurements were also taken after mixing Ag NPrs with Hyd, which verifies the interaction of nanoparticles with analyte and the enlargement of their size to 3.11 nm. The zeta potential must be investigated to comprehend and regulate the characteristics of solutions. Fig. S3 (see ESI†) depicts the average zeta potential of produced nanoparticles to be −24.5 mV. Zeta was also recorded after the combination of Ag NPrs with Hyd, and the increase of the average zeta potential to −15.5 mV indicates electrostatic interaction between the optical probe and analyte which confirms the reaction of nanoparticles with Hyd.

Considering that nanoparticles with zeta potentials higher than +30 and −30 mV have excellent stability and that increasing zeta potential leads to decreased particle aggregation and increased particle size, it can be said that the nanoparticles created here have good stability. Fig. S4 (see ESI†) displays FE-SEM images of Ag NPrs revealing a regular triangular shape. Fig. S5 (see ESI†) shows the EDS spectrum of produced nanoparticles, which reveals the presence of C, N, O, Na, and Ag in their composition. AFM was also used to examine the nanostructure's surface topology (Fig. S6 (see ESI†)). The results of the AFM supported the findings of previous characterized data.

3.1.2. Ag nanowires (Ag NWs). Several approaches were used to examine the characteristics of silver nanoparticles, including DLS to measure hydrodynamic diameter, zeta potential to investigate the surface charge, and AFM to assess three-dimensional surface topography and particle size. The results of DLS and zeta potential showed that the particles had a size of 16.16 nm (Fig. S7 (see ESI†)) and a surface charge of −30 mV (Fig. S8 (see ESI†)). DLS data and zeta potential obtained from the combination of Ag NWs and Hyd showed the particle's size grows to 115.4 nm. Also, after the interaction, the surface charge decreases to −35.5 due to the precipitation process. Those results confirmed excellent interaction of optical probe (AgNWs) with the candidate analyte (Hyd).

Fig. S9 (see ESI†) depicts FE-SEM images of AgNWs that were used to assess the surface morphology of the sample. In addition, the quality and quantity of compounds were assessed using EDS, which verified the presence of large quantities of silver in the analyzed sample (Fig. S10 (see ESI†)). Two-dimensional and three-dimensional AFM morphologies demonstrate the effective production of AgNWs (Fig. S11 (see ESI†)).

The effectiveness of photonic colorimetric chemosensors for the detection of hydrazine was assessed by UV-vis spectrophotometric method using AgNPs as optical probes are well suited for colorimetric and fluorometric detection due to their absorption peak in the visible wavelength range.[29]

3.2. UV-vis spectroscopic measurements

Initially, the UV-vis method was used to monitoring of hydrazine based on red/blue shift of wavelengths. The synthesized Ag NPrs and Ag NWs as optical probe were evaluated using the UV-vis method. The maximum absorption for Ag NPrs and Ag NWs around 633 and 427 nm, respectively, confirms its successful synthesis. As shown in the inset of Fig. 1, the addition of Hyd to the blue solution of AgNPrs tends to become colorless after 2 minutes, also the intensity of the solution bands is significantly reduced and the change of λ towards a lower spectrum for the absorption band at 558 nm. It is interesting to note that upon adding of Hyd, the pale silver color of AgNWs turns to blackish ash color. Also, the intensity of the bands increased significantly and the change of λ towards a lower spectrum for the absorption band at 400 nm occurred. Those results show that there is an electrostatic interaction between optical probes (AgNWs and AgNPrs) and analyte (Hyd). So, the proposed method is able to detection of candidate molecules using the UV-vis method. Also, the designed chemosensor has appropriate application for the naked-eye colorimetric monitoring of Hyd. It is important to point out that, there is a reverse relation on the detection process of designed optical chemosensors by AgNWs and AgNPrs. As previously mentioned, the intensity of peaks after the electrostatic interaction of Hyd with AgNPrs decreased. But, by optical probes (AgNWs), this interaction led to an increment of peak absorption.

3.3. Identifying appropriate AgNPs for Hyd detection (optimization of candidate optical probe)

Three different types of AgNPs with various morphology and size including AgNPrs, AgCit and AgNWs were synthesized and introduced into 0.01 M Hyd standard solution at a ratio of 1 : 1 to produce distinct color changes for analyte detection. As shown in Fig. 2, a clear color change was observed for the AgNWs as soon as the target analyte was added, the color changed from colorless to dark gray. Also, the AgNPrs solution

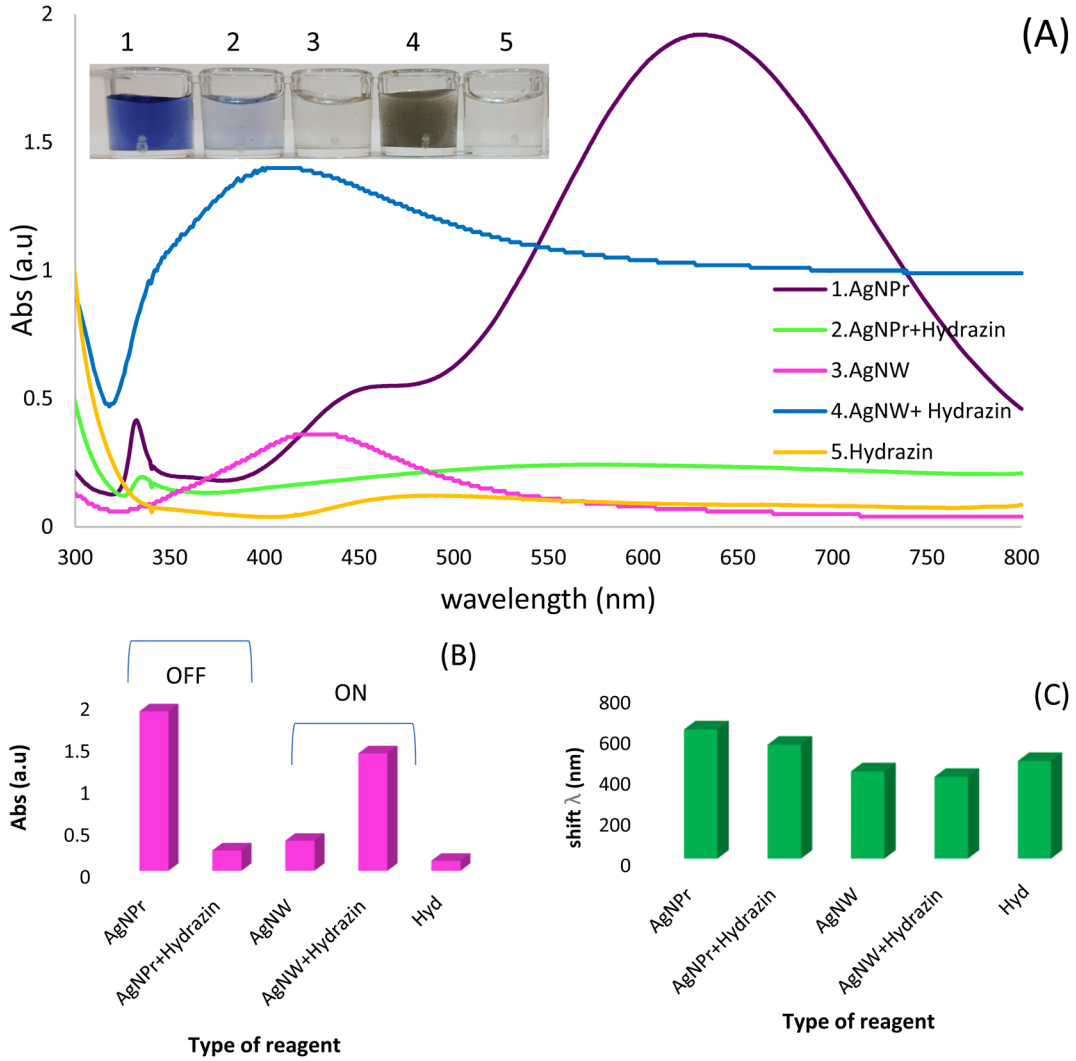

Fig. 1 (A) photographic images and Spectroscopic record: no. 1 containing 200 mL of synthesized AgNPrs aqueous solution, no. 2 a combination of a mixture of Hyd and AgNPrs in a ratio of 1 : 1, no. 3 containing 200 mL of synthesized AgNWs solution, no. 4, a mixture of Hyd and AgNWs diluted at a ratio of 1 : 1, no. 5 containing 200 mL of Hyd solution, along with their photographic images. (B) UV-vis absorption response histogram. (C) Histogram of wavelength changes *versus* the type of reagent.

changed from sea blue to colorless after one minute (reaction time) after adding the analyte. However, the combination of AgCit and Hyd had no color change. Accordingly, AgNPrs and AgNWs were selected for further investigation.

3.4 Analytical study

To evaluate the application of optical probes for the determination of various concentrations of Hyd using colorimetric and spectroscopic techniques, various concentrations of Hyd (5 to 0.02 M) in deionized water were obtained. For this purpose, AgNPrs were added to Hyd solution in a 1 : 1 ratio. These combinations were instantly photographed after 3 and 30 minutes. After 30 minutes, the concentration (0.6–5 M) of Hyd transformed the blue hue of AgNPrs to the lighter shade, and then to a colorless state that is readily visible to the naked eye. In addition, a linear relationship between UV-vis absorption peak and hydrazine concentration was observed. It is obvious that by increasing the concentration of Hyd, the absorption bands of spectrum were decrease. The results indicate that efficient interaction of Hyd with AgNPrs is dependent not only on its concentration but also on the response time (Fig. 3A). In addition, various concentrations of Hyd (ranging from 0.08 to 6 M) were prepared in deionized water. Then, 1 : 1 dilution of AgNWs with deionized water was added to them. The photographs of these combinations were taken soon after mixing. After 15 minutes, all prepared concentrations of Hyd altered the pale silver color of AgNWs to a dark gray tint. The changes in the hue and UV-vis absorption of each system depicted in (Fig. 3C) which confirm the efficacy of interaction process. Interestingly, 5 minutes after the completion of the reaction, the sediment is completely visible in the investigated solution.

Using calibration curves (Fig. 3B and D), the calculated regression equation of Hyd, Abs = 0.0801C (Hyd) + 0.5458 (R^2 = 0.9883) and Abs = 0.1254C (Hyd) + 0.4993 (R^2 = 0.98) by both

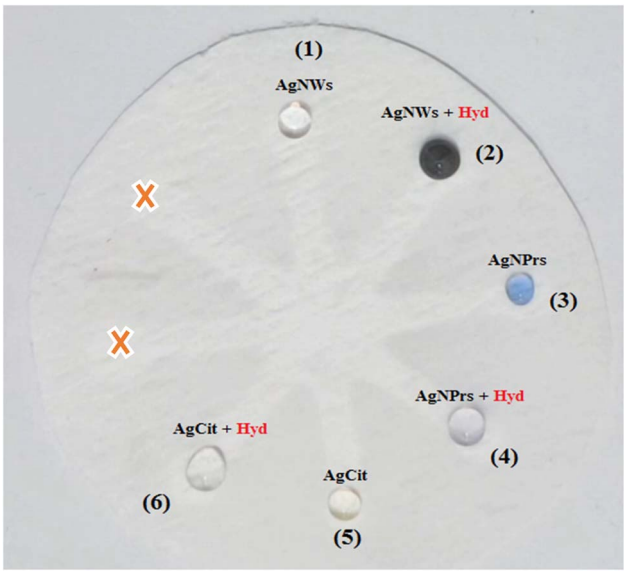

Fig. 2 Photographic images of the fiberglass microfluidic paper-based calorimetric chemosensor for Hyd detection systems: AgNWs and AgNWs-Hyd (zone 1 and 2), AgNPrs and AgNPrs-Hyd (zone 3 and 4), AgCit and AgCit-Hyd (zone 5 and 6).

AgNPrs and AgNWs as optical probes, respectively which nanoparticles verifies the linear relationship between peak absorbing and concentration of analyte.

In addition, the color change over time for different concentrations of Hyd in the presence of AgNWs and AgNPrs were recorded. Given in Fig. S12 (see ESI†)'s, UV-vis absorption and calibration plots can provide a unique way for estimating the approximate concentration of Hyd based on the time/color system.

Although UV-vis spectrophotometric results are ideally suited for Hyd determination, their application is limited and restricted to laboratories. In addition to being inexpensive, portable, and easily accessible, paper-based microfluidics do not need complicated, multi-step instrumentation like previous sensors. A paper-based chemosensor that can be manufactured in a tiny size may simultaneously assess several samples with minimal material use. Due to these benefits, this sort of substrate was utilized in the colorimetric section to detect and assess the effect of varying Hyd concentration. Microfluidic paper with a hydrophobic network and resistance to the absorption of AgNWs, Hyd, and AgNPrs was utilized for this purpose. Therefore, the injected droplet of AgNPrs and AgNWs had roughly one hour to adsorb or dry on the paper after reacting with Hyd.

As shown in Fig. 4, the wells numbered 1 through 8 were treated with 5 microliters of AgNPrs and AgNWs, followed by the addition of 5 microliters of Hyd at various concentrations. All concentrations of Hyd (10 mM–5 M dissolved in AgNPrs) exhibited color change after 1 hour, whereas the duration of color change in all concentrations of Hyd (8 mM–6 M mixed with AgNWs) was reduced to 30 minutes. This is the case due to its viscosity and surface adsorption, paper-based microfluidics

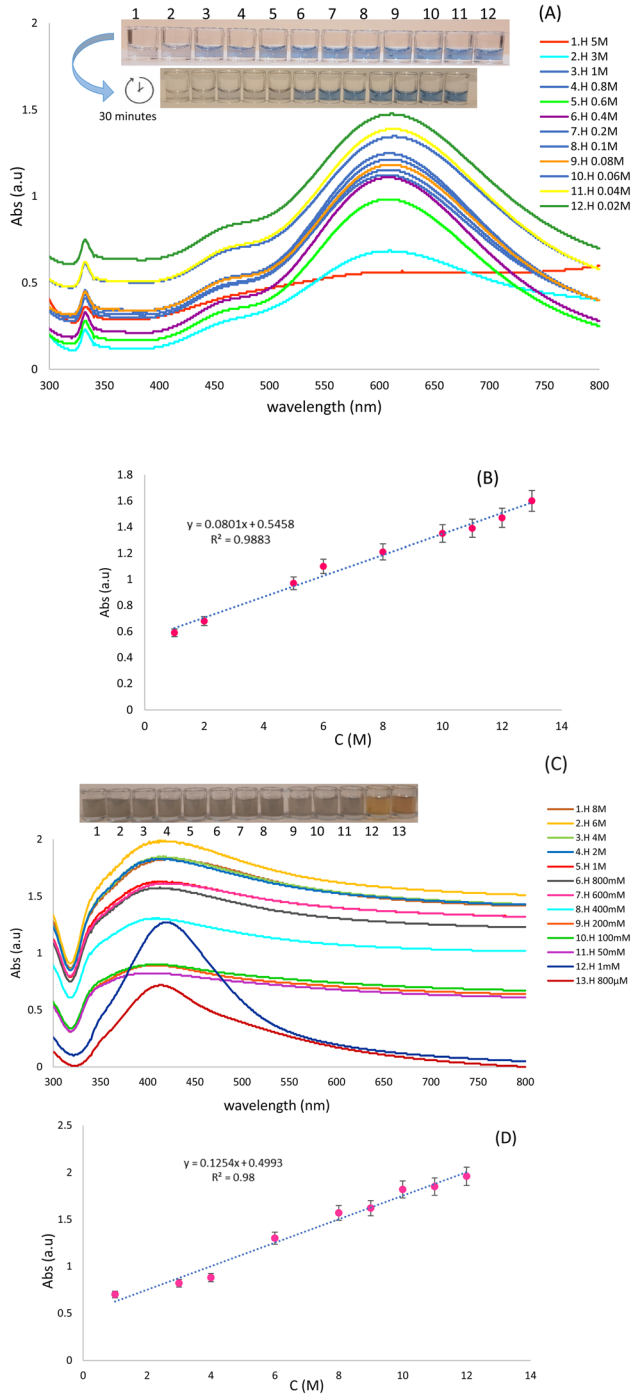

Fig. 3 (A and C) UV-vis spectra of different concentrations of Hyd in the presence of optical probes (AgNPrs, AgNWs) in 1 : 1 ratio, respectively, along with digital images. (B and D) Calibration plot of peak intensity *versus* concentration of Hyd.

results in a longer reaction time. However, the results demonstrated that the suggested platform can be employed as a commercially viable colorimetric kit for the environmental analysis of Hyd in laboratories (see Video files†).

Other current methods and strategies for detecting Hyd are detailed in Tables 1 and 2. Using AgNPrs and AgNWs, we intend to develop an analytical approach for the detection of the

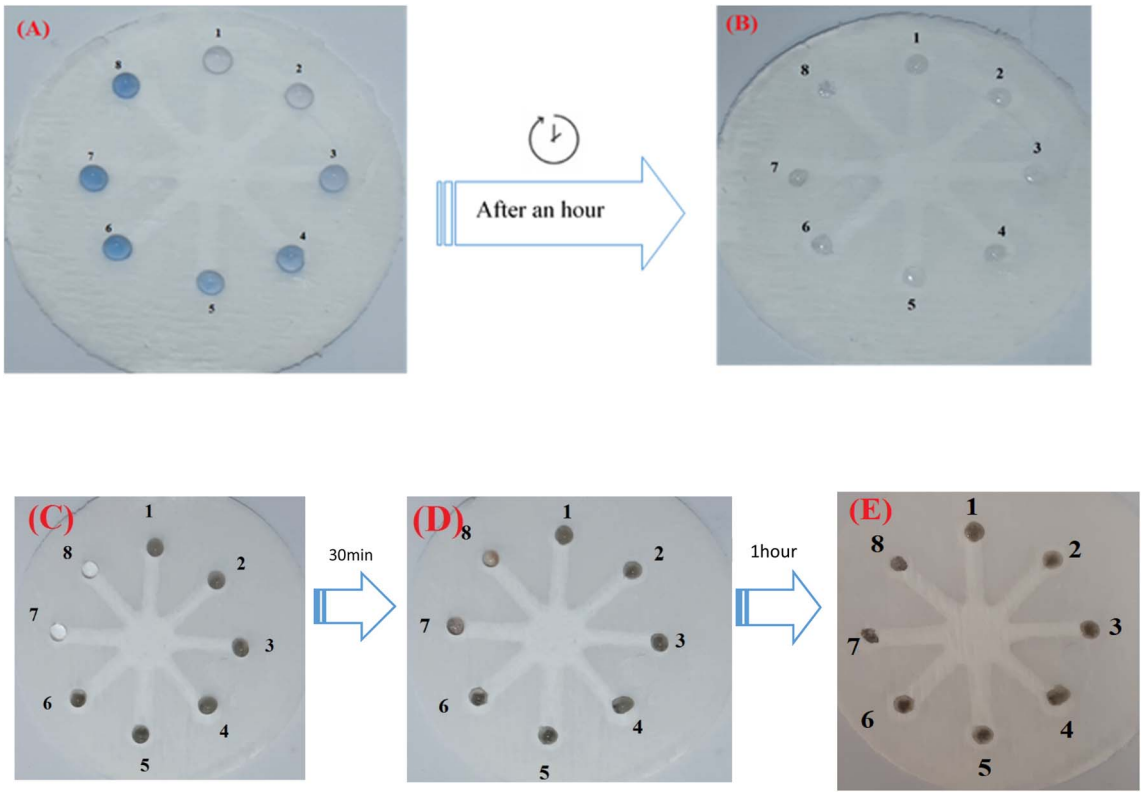

Fig. 4 Photographic images of the μPCD-based colorimetric system in the presence of: (A) AgNPs in different concentrations of Hyd (5–0.1 M) zones 1 to 8 (before), and (B) after an hour, (C) AgNWs in different concentrations of Hyd (8–0.4 M) zones 1 to 8 (before), and (D and E) after a 30 min and an hour, respectively.

hazardous chemical Hyd. Other factors such as precision, comfort, reliability, speed, and ease of use are also evaluated as qualification criteria. In addition, our results demonstrated that the analytical values of the proposed system are superior to those of earlier systems and that the reaction time is incredibly quick without the need for chromogenic reagents. In addition, the abovementioned sensors (Tables 1 and 2) require an electrical device with a power supply, the miniaturization of which necessitates additional costs and research. Therefore, we anticipate that this method will lead the way for future environmental safety experiments. Since the suggested analytical method does not require supplementary equipment, it can be

Table 1 A brief evaluation of various reported analytical optical methods for the monitoring of Hyd

Sensing method	Probe	Sample	Solvent	Time	LOD	Ref.
Fluorescence (Ratiometric/ICT) & UV-vis	Coumarin	Waste water	Acetate buffer/ DMSO (1 : 9)	40 min	2×10^{-5} M	30
Fluorescence (chemiluminescence)	Schaap's adamantylidene–dioxetane	Water samples/HeLa cells	PBS/DMSO (7 : 3)	60 min	9.3×10^{-7} M	31
Fluorescence & UV-vis	Flavone	Water samples	PBS/DMSO (1 : 9)	70 min	3.6×10^{-7} M	32
Fluorescence	Fluorescein	Tap water and distilled water, BT474 cells	HEPES/DMSO (1 : 1)	3 min	5.7×10^{-8} M	33
Fluorescence/PET	Coumarin	Water samples	PBS/DMSO (1 : 3)	3 h	0.0047 μM	34
Fluorescence (ICT)	DDPB	Biological & water samples	DMSO	20 min	86.3 nM (2.76 g L^{-1})	35
Fluorescence (ratiometric/ICT)	4-(*N*,*N*-Diphenylamino) benzaldehyde	Real water and soil samples, MC3T3 cells	HEPES/DMSO (7 : 3)	1.5 min	204 nM	36
Fluorescence (ratiometric/ESIPT)	*p*-Dimethylaminobenzaldehyde	Water samples	PBS/DMSO (1 : 1)	2 h	0.063 μM	37
UV-vis & μPCD colorimetric	Silver nanowire, silver nanoprism	Water samples	—	1^{st} second after a while	800 μM, 200 μM	This study

Table 2 A comparison between the proposed colorimetric system and previously reported methods

Analytical technique	Reaction system	LOD	Linear range	Ref.
Electrochemical	SnO_2/CeO_2/GCE	0.179 μM	3–26 μM	38
Electrochemical	CDs-Cu_2O/CuO	0.024 μM	0.99–5903 μM	39
HS-SPME/GC-MS/MS	1,1,1-Trifluoro-2,4 pentanedione (1,1,1-TFPD)	0.002 μg L^{-1}	0.011–0.074 μg L^{-1}	40
Chemiluminescent and amperometric	Bromometric titration	60 nM	2 μM–1.1 mM	41
HPLC	Benzaldehyde	0.3 μg L^{-1}	1–500 μg L^{-1}	42
UV-vis & μPCD colorimetric	Silver nanowire, silver nanoprism	800 μM, 200 μM	0.08–6 M, 0.02–5 M	This study

simply miniaturized and employed as a low-cost diagnostic device without the requirement for skilled professionals.

3.5. Analytical validation

3.5.1. Selectivity study. The interaction of AgNPrs, and AgNWs with eight types of potential interferers including formaldehyde, ethanol (EtOH), methanol (MetOH), glucose (Glu) at a concentration of 0.1 M, Ca, K, and Na ions were evaluated using UV-vis absorption and μPCD to determine the effect of possible interference of other species on selectivity of optical chemosensor. As shown in (Fig. S13 (see ESI†)) with the addition of formaldehyde, Glu, Ca, K and Na the maximum absorption wavelength of AgNPrs changed from 633 to 433, 479, 426, 433, 441 nm, respectively. Concurrently, the color of AgNPrs changed from dark blue to yellow, as shown in Fig. S13A (see ESI†). It reduces the circumference of the triangular-shaped AgNPrs' morphology. However, the absorption wavelength and color of AgNPrs in the presence of EtOH, MetOH, and acetone do not alter much. Adding a 1 : 1 ratio of Hyd and interferents to the AgNPrs solution has no discernible effect on the wavelength of AgNPrs absorption, as shown in (Fig. S13D (see ESI†)). Consequently, the data indicate that none of these species can interact appreciably with Hyd at the amounts measured. So, those species have no interfering effect on the performance of optical chemosensor of Hyd.

Interestingly, the data obtained from the UV-vis absorption spectrum and the colorimetric system following the mixing of the aforementioned interferents with AgNWs do not reveal any significant interference (Fig. S14A (see ESI†)). When examining the results of incubation of the interferents with Hyd at a ratio of 1 : 1 and it's mixing with optical probe (AgNWs), the color of AgNWs in the presence of Glu, EtOH, and MetOH changes from colorless to gray, and its spectrum changes dramatically, indicating that these interferers do not disrupt the Hyd-AgNWs detection system (Fig. S15 (see ESI†)). Nonetheless, if there is no discernible difference between the spectrum and the color of AgNWs in the presence of formaldehyde, acetone, and above-mentioned ions, these chemicals might be regarded as interference in the Hyd-AgNWs detection system (Fig. S14B (see ESI†)) (see Video files†).

3.5.2. Selectivity in the real environmental samples. To study the influence of possible interference of species on the performance of optical chemosensor in real samples (lake water) on Hyd measurement, the interaction of AgNPrs and AgNWs with the eight interferents listed in Section (4.3.1) was evaluated using prior techniques (UV-vis and colorimetric assay). The results were shown in Fig. S16 and S17 (see ESI†). Due to the dilution with the actual sample, the observed results show that interfering species except formaldehyde cannot significantly interfere with Hyd at the same concentration (see Video files†). Also, similar results were obtained in real samples which confirmed application of proposed photonic sensor towards analysis of Hyd in real environmental samples. Using colorimetric results of Fig. S17 (see ESI†), it's obvious that this portable μPCD is able to use for the detection and determination of Hyd in real samples. So, this design is a new platform for the smartphone – assisted recognition of this toxic agent in environmental samples.

3.6. Reproducibility and repeatability of optical chemosensors

Reliable biosensors must have excellent precision (repeatability and reproducibility). Repeatability is the agreement between repeated measurements of the same sample under optimal conditions, whereas reproducibility is the degree of agreement between results produced by the same method under varied settings.

Fig. S18 (see ESI†) depicts an evaluation of the repeatability of optical probe combinations with the same concentration of Hyd throughout three repetition periods. According to the obtained graphs, the height and location of the peaks are nearly identical, while the width of the peaks shows no significant variation. In addition, the average standard deviations obtained from the combination of AgNPrs and AgNWs optical probes with the target (Hyd 5 M) during three repetition periods are SD = 3.4 and SD = 5.59, respectively, indicating that the difference under the same conditions is not significant. In addition, the reproducibility of AgNPrs and AgNWs compounds with various concentrations of Hyd (5 M, 500 mM, and 500 μM) was examined across three repetition periods (Fig. S19 (see ESI†)). Despite the progressive decline in absorption band intensity, the reduction ratio was nearly identical for all three absorption bands, independent of wavelength position. In addition, the relative standard deviation for AgNPrs and AgNWs was calculated to be SD = 4.58 and SD = 4.49, respectively, demonstrating the method's outstanding repeatability.

3.7. Stability

Three-month stability tests were conducted on colloidal solutions of AgNPrs and AgNWs. Fig. S20 (see ESI†) displays the DLS data indicating that the size of AgNPrs and AgNWs

nanoparticles does not change significantly over time. In addition, an examination of the zeta potential results in Fig. S21 (see ESI†) for both colloidal solutions reveal that, despite slight numerical changes in the surface charge, there is no significant change in the position of the surface charge on the graph, which explains why the color of the probes used in the study did not change over time. In other words, the proposed probes demonstrated appropriate stability over a three-month period.

3.8. Comparison of candidate probes for the rapid analysis with Hyd kinetic study

For the first time, the optical behavior of the probes in the presence of varied concentrations of Hyd was evaluated over time in order to identify the most effective chemical sensor for rapid and precise analyte detection. As shown in Fig. S22 (see ESI†), AgNPrs nanoparticles can detect low amounts of hydrazine over an extended period of time. According to the data obtained in 80 minutes for 200 M Hyd and 10 minutes for 5 M Hyd, the color of the solution changes from dark blue to colorless. However, the color changes for AgNWs in the examined concentration range were quite rapid, so for nearly all Hyd concentration ranges, the color of the AgNWs solution changed from pale silver to blackish gray in around 15 minutes. In addition, based on the logarithmic equations obtained from Fig. S22 (see ESI†), we found that the time variations *versus* Ln of hydrazine concentrations may be accurately characterized ($R_{AgNPrs}^2 = 0.9567$, $R_{AgNWs}^2 = 0.9848$). Comparing the vertical intercept (+25.863 and +6.5875) for AgNPrs and AgNWs demonstrates that AgNPrs, which have a wider vertical intercept than AgNWs, require a longer time to see the color change in the presence of the analyte. The slope of the line, which also demonstrates the sensitivity of concentration changes with respect to time, demonstrates that AgNPrs with a line slope of (−12.96) require more time for minor concentration changes than AgNW with a line slope of (−1.947). However, due to the quick kinetics of AgNWs, AgNPrs nanoparticles are capable of detecting low amounts of hydrazine.

4. Conclusion

In this study, the identification of hydrazine was assessed using three distinct silver nanomaterials: silver nanoprism (Ag NPrs), silver nanowire (Ag NW), and Ag-Cit NPs. Since AgNW and AgNPrs produced outstanding colorimetric outcomes, they were fully investigated for the qualitative and quantitative analysis of Hyd. The acquired analytical results for the suggested colorimetric chemosensor based on AgNWs (optical probe) are quite faster than those of existing systems. In addition, AgNW and AgNPrs were able to detect hydrazine in environmental aquatic samples. In the final phase of this project, the reported μPCD was adjusted for colorimetric system integration. This optimization made it possible to provide a unique analytical method based on the time/color characterization of each hydrazine concentration. Additionally, the selectivity tests for developed systems were appropriate, and the stability of AgNW and AgNPrs for at least 90 and 60 days, respectively, was proven which makes commercialization of the suggested system more feasible. In addition to the simple, rapid, and sensitive colorimetric and spectrophotometric recognition system of hydrazine, this study provides a novel portable platform for the monitoring of Hyd in real samples using optical chemosensing approach.

Conflicts of interest

There are no conflicts to declare.

Acknowledgements

We are grateful for the financial assistance of this work from the Tabriz University of Medical Sciences, Pharmaceutical Analysis Research Center (Grant No. 69057, Ethic No. IR.TBZMED.VCR.REC.1401.142).

References

1 N. F. Atta, A. Galal and A. R. El-Gohary, *J. Electroanal. Chem.*, 2021, **888**, 115165.
2 L. Yan, S. Zhang, Y. Xie, X. Mu and J. Zhu, *Crit. Rev. Anal. Chem.*, 2022, **52**, 210–229.
3 P. D. Tzanavaras, S. Themistokleous and C. K. Zacharis, *J. Pharm. Biomed. Anal.*, 2020, **177**, 112887.
4 S. D. Hiremath, R. U. Gawas, D. Das, V. G. Naik, A. A. Bhosle, V. P. Murali, K. K. Maiti, R. Acharya, M. Banerjee and A. Chatterjee, *RSC Adv.*, 2021, **11**, 21269–21278.
5 S. Subburaj, B. Arumugam, S.-M. Chen, T.-W. Chen, A. Seetharam and S. K. Ramaraj, *Int. J. Electrochem. Sci.*, 2021, **16**, 19–24.
6 A. Afsharas, I. Tsyrulneva and O. Zaporozhets, *Methods Objects Chem. Anal.*, 2015, **10**, 97–107.
7 H. N. Nguyen MC USAF, J. A. Chenoweth, V. S. Bebarta MC USAF, T. E. Albertson and C. D. Nowadly MC USAF, *Mil. Med.*, 2021, **186**, e319–e326.
8 Y. Ding, S. Zhao, Q. Wang, X. Yu and W. Zhang, *Sens. Actuators, B*, 2018, **256**, 1107–1113.
9 M. I. Khan, M. Tayyab, M. M. Hassan, N. Muhammad, A. Ahmad, M. Tariq and A. Rahim, *Toxic Gas Sensors and Biosensors*, 2021, vol. 92, pp. 139–156.
10 J. Wang, C. Wang, S. Jiang, W. Ma, B. Xu, L. Liu and W. Tian, *J. Mater. Chem. C*, 2022, **10**, 2807–2813.
11 X.-Y. Zhang, Y.-S. Yang, W. Wang, Q.-C. Jiao and H.-L. Zhu, *Coord. Chem. Rev.*, 2020, **417**, 213367.
12 E. Saeb and K. Asadpour-Zeynali, *Microchem. J.*, 2021, **160**, 105603.
13 G. Choudhary and H. Hansen, *Chemosphere*, 1998, **37**, 801–843.
14 R. Singh, P. Thakur, A. Thakur, H. Kumar, P. Chawla, J. V. Rohit, R. Kaushik and N. Kumar, *Int. J. Environ. Anal. Chem.*, 2021, **101**, 3006–3022.
15 M. P. Bhat, M. Kurkuri, D. Losic, M. Kigga and T. Altalhic, *Anal. Chim. Acta*, 2021, **1159**, 338439.
16 V. Brahmkhatri, P. Pandit, P. Rananaware, A. D'Souz and M. D. Kurkuri, *Trends Environ. Anal. Chem.*, 2021, **30**, e00117.

17 G. Xu, N. Guo, Q. Zhang, T. Wang, P. Song and L. Xia, *J. Hazard. Mater.*, 2022, **424**, 127303.
18 Y. Chen, W. Mo, Z. Cheng, F. Kong, C. Chen, X. Li and H. Ma, *Dyes Pigm.*, 2022, **198**, 110004.
19 L.-J. Yan, C. Jiang, A.-Y. Ye, Q. He and C. Yao, *Spectrochim. Acta, Part A*, 2022, **268**, 120639.
20 Q. Kong, Y. Wang, L. Zhang, S. Ge and J. Yu, *Sens. Actuators, B*, 2017, **243**, 130–136.
21 A. K. Ellerbee, S. T. Phillips, A. C. Siegel, K. A. Mirica, A. W. Martinez, P. Striehl, N. Jain, M. G. Prentiss and G. M. Whitesides, *Anal. Chem.*, 2009, **81**, 8447–8452.
22 P. Lin, S. W. Kwok, Y. H Lin, V. Singh, L. Kimerling, G. M. Whitesides and A. Agarwal, *Nano Lett.*, 2014, **14**, 231–238.
23 M. M. Hamedi, A. Ainla, F. Guder, D. C. Christodouleas, M. T. Fernandez-Abedul and G. M. Whitesides, *Adv. Mater.*, 2016, **28**, 5054–5063.
24 C. Walgama, M. P. Nguyen, L. M. Boatner, I. Richardsb and R. M. Crooks, *Lab Chip*, 2020, **20**, 1648–1657.
25 J. J. Yoo, M. J. Anderson, T. M. Alligrant and R. M. Crooks, *Anal. Chem.*, 2014, **86**, 4302–4307.
26 H. Liu and R. M. Crooks, *J. Am. Chem. Soc.*, 2011, **133**(44), 17564–17566.
27 F. Farshchi, A. Saadati, M. Hasanzadeh and F. Seidi, *RSC Adv.*, 2021, **11**, 27298–27308.
28 W. Wang, S. Ding, Z. Wang, Q. Lv and Q. Zhang, *Biosens. Bioelectron.*, 2021, **187**, 113310.
29 S. K. Manna, A. Gangopadhyay, K. Maiti, S. Mondal and A. K. Mahapatra, *ChemistrySelect*, 2019, **4**, 7219–7245.
30 K. Li, H.-R. Xu, K.-K. Yu, J.-T. Hou and X.-Q. Yu, *Anal. Methods*, 2013, **5**, 2653–2656.
31 J. Liu, J. Jiang, Y. Dou, F. Zhang, X. Liu, J. Qu and Q. Zhu, *Org. Biomol. Chem.*, 2019, **17**, 6975–6979.
32 X. Zhang, C. Shi, P. Ji, X. Jin, J. Liu and H. Zhu, *Anal. Methods*, 2016, **8**, 2267–2273.
33 W.-Z. Xu, W.-Y. Liu, T.-T. Zhou, Y.-T. Yang and W. Li, *Spectrochim. Acta, Part A*, 2018, **193**, 324–329.
34 X. Jiang, Z. Lu, M. Shangguan, S. Yi, X. Zeng, Y. Zhang and L. Hou, *Microchem. J.*, 2020, **152**, 104376.
35 M. Zhu, Y. Xu, L. Sang, Z. Zhao, L. Wang, X. Wu, F. Fan, Y. Wang and H. Li, *Environ. Pollut.*, 2020, **256**, 113427.
36 S. K. Samanta, K. Maiti, S. S. Ali, U. N. Guria, A. Ghosh, P. Datta and A. K. Mahapatra, *Dyes Pigm.*, 2020, **173**, 107997.
37 C. Wu, H. Xu, Y. Li, R. Xie, P. Li, X. Pang, Z. Zhou, H. Li and Y. Zhang, *Anal. Methods*, 2019, **11**, 2591–2596.
38 A. Mohammad, M. E. Khan, I. M. Alarifi, M. H. Cho and T. Yoon, *Microchem. J.*, 2021, **171**, 106784.
39 G. Wei, L. Wang, L. Huo and Y. Zhang, *Talanta*, 2020, **209**, 120431.
40 J.-A. Oh and H.-S. Shin, *Anal. Chim. Acta*, 2017, **950**, 57–63.
41 Z. He, B. Fuhrmann and U. Spohn, *Anal. Chim. Acta*, 2000, **409**, 83–91.
42 Y. V. Timchenko, A. Apenkina, A. Smolenkov, A. Pirogov and O. Shpigun, *J. Anal. Chem.*, 2021, **76**, 1163–1171.